

ARTICLE

OPEN



Impact of a Mn-oxidizing bacterial strain on the dissolution and browning of a Mn-bearing potash-lime silicate glass

Valentina Valbi¹✉, Anne Perez¹, Aurélie Verney-Carron² and Stéphanie Rossano¹

This work aims to investigate the role played by a model Mn-oxidizing bacterial strain and its exudates on the alteration of Mn-bearing potash-lime silicate glasses representative of medieval stained glass windows. Two model glasses, with or without manganese, were prepared and used for abiotic and *Pseudomonas putida* inoculated dissolution experiments. Results show that the presence of *P. putida* slows down the dissolution kinetics while changing the dissolution stoichiometry. In biotic experiments, the acidification of the solution at the beginning of the experiment favors the release of K. After a few days, a drop in Mn and P in solution is observed, retained by bacterial cells. Reciprocally, the amount of glass influences bacterial behavior. The more glass, the faster the bacterial population increases in size and produces siderophore. In the presence of the Mn-bearing glass, siderophore production is followed by the formation of brown phases, identified as Mn oxides.

npj Materials Degradation (2023)7:20; <https://doi.org/10.1038/s41529-023-00338-5>

INTRODUCTION

In the Middle Ages, the use of a flux provided by vegetal ash (beech and fern) lead to the production of stained glass with a lower silica content and a high calcium and potassium content^{1,2}. Due to their compositions, these glasses are especially sensitive to the effect of the environment and develop alterations caused by the exposure of the glass to the combined action of water, climate, pollution and microorganisms^{2–9}.

The browning phenomenon is a pathology that specifically concerns stained glasses containing manganese. Manganese can be present at concentration around 1–2 MnO wt% in archaeological glass and stained glass windows due to its use either as a chromophore to obtain purple shades or as a decolorizer^{10–15}. The browning phenomenon has been detected on several stained glass windows in Northern Europe and on numerous archaeological samples. It results in the presence of brown stains on the surface of the glass, which can cause a loss in light transmission, and, therefore, legibility of the work. These brown spots are rich in Mn (III, IV) and are located in the altered layer of the glass^{16–21}.

Several works consider that the Mn-related brown coloration is due to a microbiological effect^{22–25}. Mn is a micronutrient for some microorganisms and several of them are known to produce brown or black oxides from Mn present in the environment^{26–30}. In addition, the browning exhibits surface morphology in the form of craters, which is often associated with microbiologically-driven alterations^{22–24,31–33}. These observations support the hypothesis that the formation of brown phases rich in Mn might be related to the action of microorganisms. Yet, there is no experimental evidence that shows a direct implication of microorganisms in the appearance of the browning phenomenon in medieval stained glass.

Bioalteration occurs through the interaction of microorganisms and the surface of an inorganic solid (mineral or glass) which leads to a physicochemical degradation of the latter. In the environment, microorganisms can influence the dissolution of oxides, minerals and glasses by direct contact of the cells to the surface, i.e. by constituting biofilms, or indirectly through the local change of pH

and redox conditions or through the production of metabolites such as low molecular weight organic acids and siderophores that will interact with the elements constituting the surface of the solid substrate^{34–46}. Siderophores are molecules widely produced by microorganisms in order to increase the bioavailability of nutrient elements because of their chelating properties. They are tetradentate or hexadentate chelating ligands that contain different functional groups, alone or combined, such as hydroxamate, catecholate, and carboxylate binding moieties arranged in linear or not linear configurations⁴⁷. Siderophores are mostly known for their Fe-chelating ability, but they also strongly complex other elements such as Mn, Co and Cr^{48–50}. Some studies investigated the effect of bacteria on the dissolution of different minerals, such as hornblende^{35,51–53}, kaolinite⁵⁴, olivine⁵⁵, smectite⁵⁶, biotite⁴⁶ or diopside⁵⁷, and some of them specifically focused on the role of siderophores in the process^{35,51–53,56}.

Concerning glass bioalteration, a few studies investigated the effect of living microorganisms on glass weathering by describing the observable effects of bio-attacks on the glass surface, such as micropitting and cracking due to fungal hyphae^{24,31,58}. Other research groups in the field of environmental sciences carried out biodissolution experiments in order to understand the underlying dissolution mechanisms involving acidification and/or complexation through chelating molecules^{43,45,53,59–62}. Most of these biodissolution studies were dedicated to natural glasses and minerals; to the authors' knowledge, none of them focused on artificial cultural heritage glasses.

In a previous work⁶³, the indirect effect of microorganisms on glass dissolution was studied with a specific focus on the impact of biogenic exudates (oxalic acid (OA) and the siderophore DFOB) on the dissolution of model Mn-bearing and Mn-free potash-lime-silicate glasses representative of the composition of medieval stained glasses. That work showed that both OA and DFOB increase the dissolution rate of the glass through different mechanisms (mainly proton-promoted mechanism for OA and ligand-promoted mechanism for DFOB), more or less accentuated depending on the glass composition (Mn presence or absence).

¹Laboratoire Géomatériaux et Environnement, Univ Gustave Eiffel, F-77454 Marne-la-Vallée, France. ²Univ Paris Est Creteil and Université Paris Cité, CNRS, LISA, F-94010 Créteil, France. ✉email: valentinavalbi@gmail.com

The aim of the present work is to study the direct effect of bacteria on the dissolution of the same model glasses. We investigate the dissolution behavior of two model potash-lime-silicate glasses (with or without manganese, VM and VNM) in different experimental conditions involving a model bacteria strain, as well as the bacteria behavior in response to the elements released from the glass. *Pseudomonas putida* was chosen as a model strain because it is easily cultivable and it is a widely studied strain in literature, especially for its Mn-oxidizing properties and siderophores production^{64–67}, thus making it a suitable model strain for this work. It is a heterotrophic and non-pathogen strain, belonging to the *Pseudomonas* genus, often used in biodissolution studies of minerals and natural glasses^{43,45,56,61,62}. The possible interactions of *Pseudomonas putida* with the glass elements are discussed.

RESULTS

Different alteration experiments were performed in 200 mL of liquid culture (ultrapure water, HEPES buffer, plus carbon and nitrogen sources) with the Mn-bearing VM glass (100 mg, 50 mg, 25 mg) and the Mn-free VNM glass (100 mg), and/or *Pseudomonas putida* for 8 or 13 days (see methods). Solutions were analyzed using ICP-OES and UV-VIS spectroscopy. Bacterial growth was monitored by Optical Density (OD) measurements and plate counting. The recovered bacteria pellets were washed and mineralized, the resulting solutions analyzed by ICP-OES (Fig. 1) in order to determine the composition of the pellets and the adsorbed elements.

Bacterial growth

For all the VM biodissolution experiments, a considerable amount of biofilm was produced. As it was not possible to quantify the mass of biofilm because it was adherent to the glass powder and to the walls of the Erlenmeyers, the bacterial growth was estimated through bacterial cells in their planktonic form, using CFU counting and OD measurements at 600 nm of

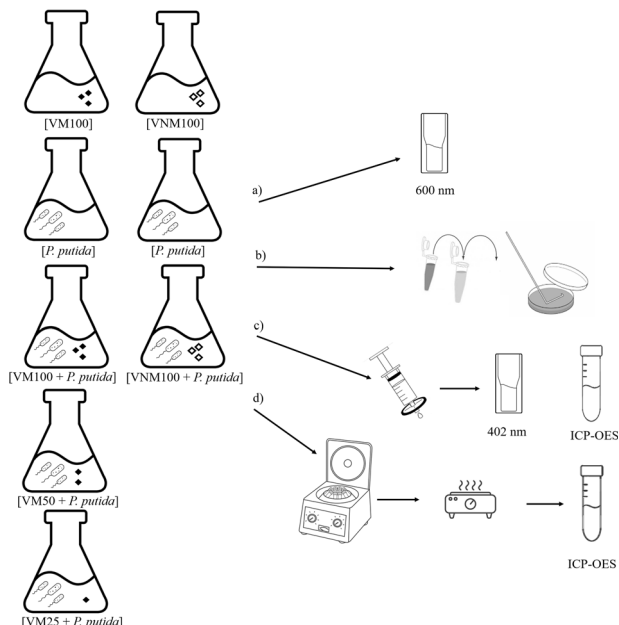


Fig. 1 Schematic experimental design of all the tested dissolution conditions and following analysis. **a** Optical Density at 600 nm, **b** plate counting by sequential dissolution, **c** UV-VIS absorption of the filtered leachates, and **d** analysis of the recovered bacterial pellets and cleaning solutions.

bacterial medium aliquots. The resulting growth curves are displayed in Fig. 2a, b).

Figure 2a shows that for the *[P. putida]* experiment, the OD values do not increase and stay below 0.3 (unitless) for the whole experiment. By contrast, there is an increase in OD values with time for all the experiments with glass during the first 3 days, then a plateau is observed. Final OD values reach 0.9, 0.13, and 0.14 for the *[VM25 + P. putida]*, *[VM50 + P. putida]* and *[VM100 + P. putida]* experiments, respectively. Despite the similar final OD values for the experiments with 50 and 100 mg of VM glass, a significant difference can be observed in the trend of the curve, with higher ODs observed for the *[VM100 + P. putida]* experiment since the first day of experiment.

The OD values for the *[P. putida]* and the biodissolution experiment with 100 mg of VM glass are also reported in Fig. 2a. The bacterial growth curves obtained in these two biodissolution experiments are almost overlapped, with slightly smaller values for the VNM glass.

The results of plate counting plotted in Fig. 2b confirm the trends observed by OD measurements despite the elevated uncertainty bars. The R^2 values calculated by plotting the OD measurements versus the CFU measurements varies between 0.8 and 0.9, thus confirming that the two methods of estimation of the bacterial growth are in good agreement.

Chromatic variations of the altering solutions and microscopic observations of the altered powder

Chromatic variations were observed with time in the bacterial media (cf. Supplementary Figs. 1, 2).

For the VNM glass, a green/yellowish hue was visible after 2 days in the *[VNM100 + P. putida]* experiment, getting more and more intense until the end of the experiment. On the contrary, both *[VNM]* and *[P. putida]* experiments kept their initial status of turbidity and color until the end of the experiments. The same results were obtained on the replicate series of experiments.

For the VM glass, an intense green hue was observed as well after 2 days for the *[VM100 + P. putida]*, that turned into brown at the third day. For the *[VM50 + P. putida]* the brown color was observed at the 6th day, and for the *[VM25 + P. putida]* a green/yellowish hue was observed at the 7th day and the browning at the 8th day. Both *[VM]* and *[P. putida]* experiments kept their initial status of turbidity and color until the end of the experiments. The same results were obtained on the replicate series but with a 1-day delay. A summary of the color evolution of the solutions is reported in Table 1.

The altered glass powder recovered at the end of the experiments and observed using optical microscopy showed that, in presence of bacteria, the VNM glass kept its whitish coloration, while the VM glass turned from purple to brown (Fig. 3a). The SEM (Scanning Electron Microscopy) observations (Fig. 3b) evidenced a thick altered layer, fractured and flaking for all the altering conditions observed. For the VM glass powders altered in presence of bacteria, the glass is partially covered with a biofilm and the EDX (Energy Dispersive X-ray analysis) mapping shows a Mn enrichment associated to the biofilm (Supplementary Fig. 3). No biofilm was observed on the VNM glass altered in presence of bacteria.

Siderophore production

The pyoverdine siderophore can be detected at 402 nm^{43,45,64,65}. The UV-VIS absorption values at 402 nm of the filtered medium aliquots are reported versus time in Fig. 4. For the *[VM100 + P. putida]* experiment, it is possible to detect the production of PVD since the first day of experiment. The absorption at 402 nm reaches a peak after 3 days, and then decreases. For the *[VM50 + P. putida]* experiment, the production of PVD starts between the first and the second day and keeps increasing slowly

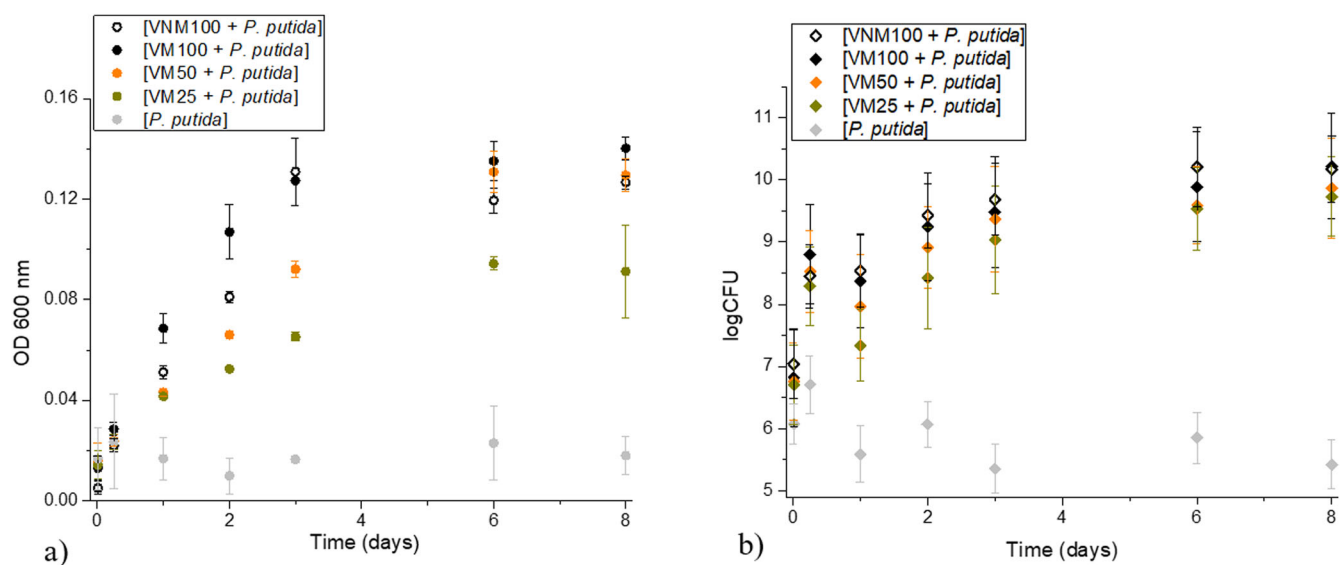


Fig. 2 Bacterial growth curves for all the biotic conditions tested. **a** Optical density measurements at 600 nm and **b** plate counting measurements. Uncertainty bars for the OD measurements correspond the standard deviation for the two set of experiments. Uncertainty bars for the CFU take into account both the standard deviation for the two set of experiments and the analytical error on the counting procedure. The R2 calculated by plotting the OD measurements versus the CFU measurements (data in SM) varies between 0.8 and 0.9.

Table 1. Summary of the results obtained. Color evolution of the solution, time of Mn drop in solution, presence of biofilm and pH values at the end of the experiment (8 days), initial dissolution rates (r_{Si}).

	Color of the solution				Drop of Mn in solution	Biofilm at the end of the experiment	pH at the end of the experiment	r_{Si} (g/m ² /d)
	At 2 days	At 3 days	At 6 days	At 8 days (end)				
[VM100]	Colorless	Colorless	Colorless	Colorless	Not observed	Not observed	7.4 ± 0.0	1.87 ± 0.49
[VM100 + <i>P. putida</i>]	Yellow/green	Brown	Dark brown	Dark brown	After 2 days	Observed	7.2 ± 0.1	0.90 ± 0.29
[VM50 + <i>P. putida</i>]	Light yellow	Light yellow	Brown	Brown	After 3 Days	Observed	6.8 ± 0.1	
[VM25 + <i>P. putida</i>]	Light yellow	Light yellow	Light yellow	Light brown	After 6 Days	Observed	6.4 ± 0.1	
[VNM100]	Colorless	Colorless	Colorless	Colorless	Not observed	Not observed	7.4 ± 0.1	1.50 ± 0.15
[VNM100 + <i>P. putida</i>]	Light yellow	Light yellow	Light yellow	Light yellow	Not observed	Not observed	7.0 ± 0.0	0.89 ± 0.12
[<i>P. putida</i>]	Colorless	Colorless	Colorless	Colorless	Not observed	Not observed	5.8 ± 0.3	

Standard deviations represent the experimental uncertainties calculated on the two set of experiments. Initial pH was 6.5 ± 0.1 for all conditions and all the solutions were colorless at the beginning of the experiment.

until the end of the experiment with final values of absorbance 3 times smaller than for the [VM100 + *P. putida*] experiment. For the [VM25 + *P. putida*] experiment, the PVD production starts between 6 and 8 days of experiment. The values for the [*P. putida*] experiment are reported as well and no production of PVD is detected over the whole experiment. The production of PVD during the [VNM100 + *P. putida*] experiment starts between 1 and 2 days and is characterized by lower absorbance values than the [VM100 + *P. putida*] experiment until the third day of experience, then it keeps increasing slowly without the significant decrease observed for the [VM100 + *P. putida*] experiment after 3 days.

A supplementary experiment [VM100 + *P. putida*] was carried out with additional samplings in order to follow the evolution of the PVD spectra over time and was run until 13 days. The results in Fig. 4b show that the recorded spectra change significantly over the course of the experiment. At the beginning of the experiment, the spectrum shows a weak absorbance around 370 nm. After 2 days, the total absorbance increases and two shoulders can be recognized, at 380 nm (A) and 410 nm (B). Then, the total intensity of the spectrum increases but the intensity ratio between the two peaks changes with the disappearance of the 380 nm peak (A).

After 3 days of experiment, the maximum intensity of absorbance is observed, and the peak at 410 nm (B) shifts toward higher wavelengths with a decrease in absorbance observed within 8 h (curve at 3.3 days). The shift of the peak (B) in the absorption spectrum, associated to a decrease in intensity in a short time is attributed to the complexation of Mn by the PVD⁶⁵. The PVD-Mn(III) complex has indeed a higher absorption λ and a weaker molar absorption coefficient ϵ than the free PVD^{64,65}. Then, the intensity of this peak (B) keeps decreasing, and a new broad peak is observed around 335 nm (C) after 6 days, and it keeps increasing until the last measurement at 13 days of experiment. The peak observed at the end of the experiment at 335 nm (C) is attributed to a degraded form of the PVD⁶⁵.

It is possible to estimate the amount of PVD produced thanks to the Beer-Lambert law and the molar absorption coefficient ϵ of the free PVD ($19,000 \text{ M}^{-1} \text{ cm}^{-1}$) reported in the literature^{64,65}. The maximum PVD concentration obtained is around $10 \mu\text{M}$ for the [VM100 + *P. putida*] experiment after 3 days and for [VNM100 + *P. putida*] after 6 days, while it is around $2 \mu\text{M}$ for both the [VM50 + *P. putida*] and the [VM25 + *P. putida*] experiments at day 6.

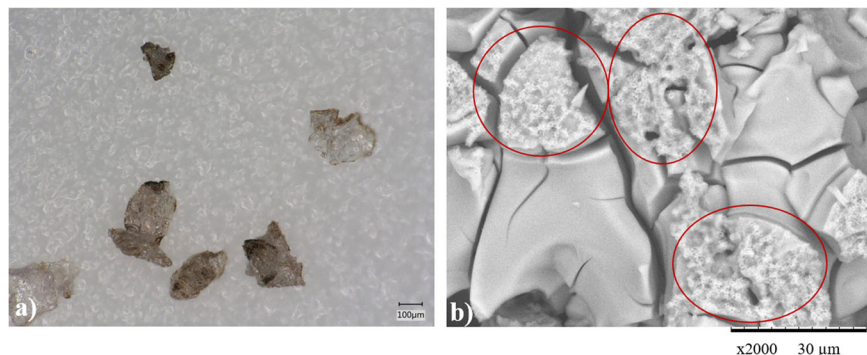


Fig. 3 Altered glass powders from the [VM100 + *P. putida*] dissolution experiment. **a** Optical microscopy and **b** scanning electron microscopy. The red circles underline the presence of biofilm.

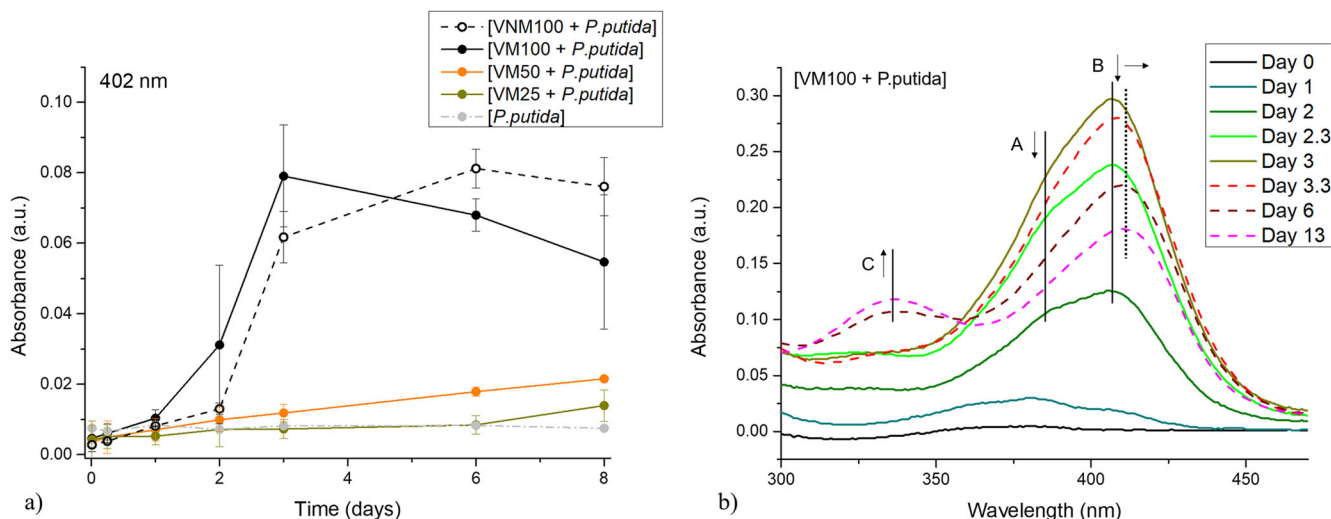


Fig. 4 UV-VIS absorption results. **a** Measurements at 402 nm, plotted versus time for all the biotic conditions tested, uncertainty bars correspond the standard deviation for the two set of experiments. **b** Absorption spectra (300–500 nm) obtained at different altering times for the 13-day experiment of [VM100 + *P. putida*].

pH and elemental concentration of the solution

The initial pH of the medium was of 6.5 ± 0.1 . The final pH was measured at the end of the experiments and the mean values are reported in Table 1. Despite the presence of the HEPES buffer, the pH evolved during the dissolution experiments. The highest pH values (around 7.4) are observed for the glass control experiments [VM100] and [VNM100], while the lowest pH values (around 5.8) are observed for the [*P. putida*] experiment. Intermediate values are obtained for the biodissolution experiments with glass and bacteria; among them, highest pH values are linked to larger amounts of dissolved glass. This rise in pH can be explained by the interdiffusion mechanism occurring during glass alteration^{9,68,69}.

Regarding all the experiments, the maximum concentration values reached 180 ppb for Al, 48 ppm for Ca, 67 ppm for K, 9 ppm for Mg, 5 ppm for Mn, and 6 ppm for P. Si concentrations reached a maximum of 36 ppm, which is still under the saturation point of amorphous silica in water (54 ppm). Generally, the values of K, Mg, Ca, and Si increase with time for all the conditions tested. In the presence of bacteria, the concentration values of P start increasing, then decrease (after one day for [VM100 + *P. putida*]) and then start increasing again. Mn concentrations increase with time and keep increasing in sterile conditions, while when in the presence of bacteria Mn amount in solution decreases after different times depending on the amount of glass in solution (2 days for [VM100 + *P. putida*]). The Mn concentrations is below

the detection limits of the spectrometer at the end of the [VM100 + *P. putida*] experiment. For the [*P. putida*] experiment, the concentrations of all the elements in solution are constant over the whole duration of the experiment.

Glass normalized mass losses

The average normalized mass losses for all the experiments containing glass are reported as a function of time in Fig. 3. In the glass abiotic conditions [VM] and [VNM], both glasses have similar behaviors and NLs of the same order of magnitude (Fig. 5a, b). The composition of the solutions indicate an incongruent dissolution: K, Ca, Mg, and P are preferentially released and follow the same evolution. The NLs of Al have low values that remain close to zero during the whole experiment. For VM glass, Mn is preferentially released compared to Si, but its dissolution curve is below those of K, Ca, Mg, and P.

In the presence of *P. putida* with 100 mg of glass (Fig. 5c, d), both glasses are characterized by a change in dissolution stoichiometry for Si, P, and Mn (for the Mn-bearing glass) compared to the abiotic [VM100] and [VNM100] experiments (Fig. 5a, b). The NLs of Si remain close to zero until 2 days for [VNM + *P. putida*] and until 1 day for [VM + *P. putida*], then they slowly rise. The NLs of P here are very low (between 5 and 10 g m^{-2}) compared to the sterile condition (until 25 g m^{-2}). For both glasses, the P concentration rises slightly at the beginning of

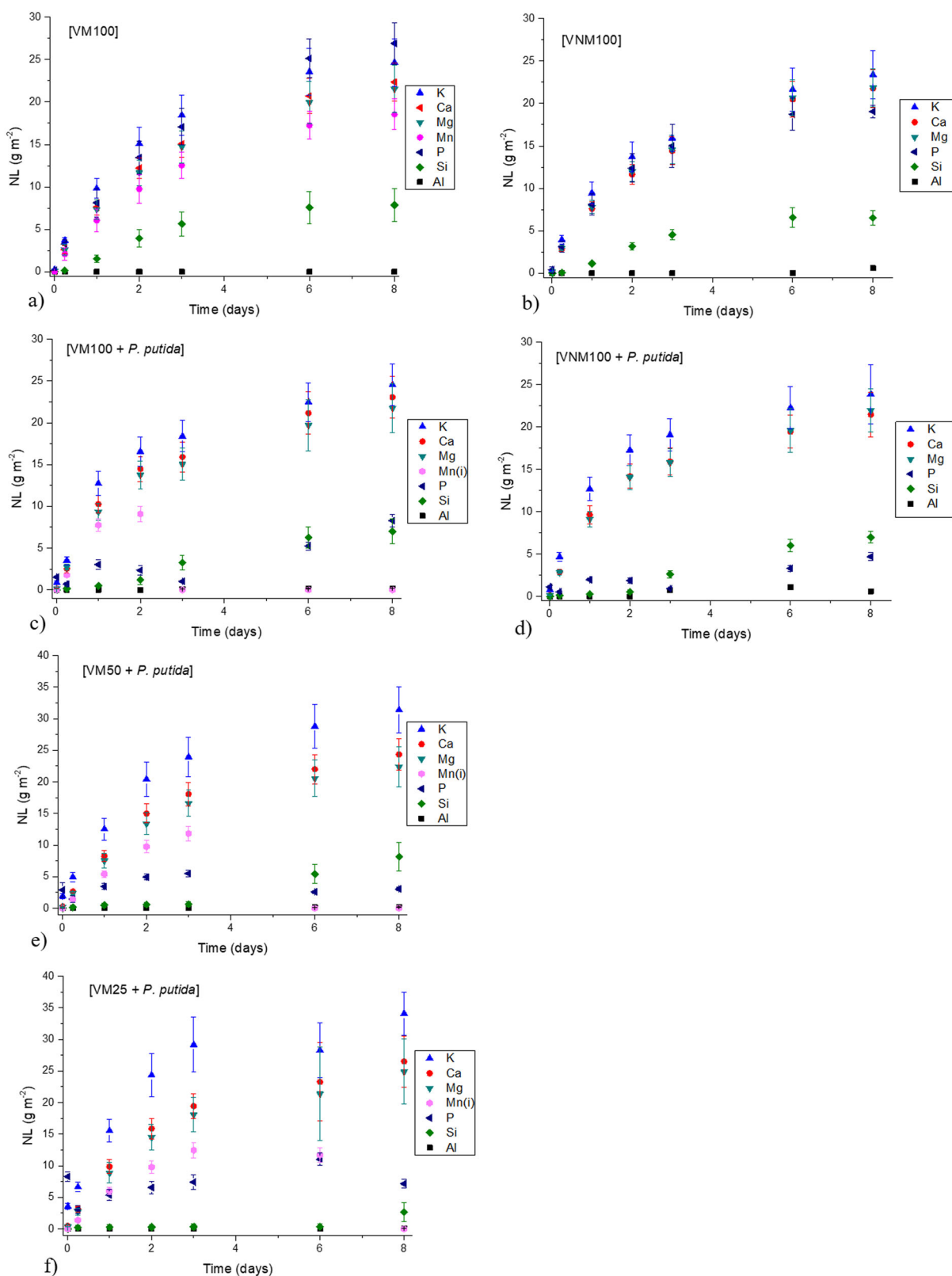


Fig. 5 Average normalized mass losses versus time. Experiments **a** [VM100], **b** [VNM100], **c** [VM100 + *P. putida*], **d** [VNM100 + *P. putida*], **e** [VM50 + *P. putida*], **f** [VM25 + *P. putida*]. Uncertainty bars correspond to the uncertainties calculated taking into account the analytical ICP-OES error (10%), and the standard deviation for the replicates.

the experiment, then falls and rises again at the end of the experiment. The Mn curve follows the same evolution as in the [VM100] during the first days of the experiment, then the NLs drop. This decrease begins after 2 days of solution exposure, and the corresponding NLs reduce to values close to zero in the following day. With regard to the experiments of dissolution of VM with a different S/V ratio (Fig. 5e, f), K, Ca, Mg behave in a different way than in the [VM100]. The NLs of Si remain below the detection limits of the spectrometer up to 3 days for [VM50 + *P. putida*] and up to 6 days for [VM25 + *P. putida*]. The evolution of P is the same for all S/V tested, but it reaches the highest NLs in the first 3 days of alteration for [VM50 + *P. putida*] and [VM25 + *P. putida*]. The evolution of Mn is also similar for all S/V but the drop in NLs (after 3 days for [VM50 + *P. putida*] and between 4 and 6 days for [VM25 + *P. putida*]) is less marked for the experiments with 50 and 25 mg of glass compared to the experiment with 100 mg.

The NLs of the two glasses have equivalent values and evolutions in abiotic conditions and in the presence of *P. putida* (Fig. 5), with the exception of the first days of experiments. The NL values of Si in the presence of bacteria seems to start increasing from 2 days, while in control glass conditions, the Si in solution starts to rise from the first day. A plateau is reached after 6 days. In the same way, P in glass control conditions has an increasing dissolution curve until a plateau is reached after 6 days. In the presence of bacteria, the NLs of P rise at the beginning of the experiment, then fall between 1 and 2 days and start to rise again. The increase of the NL values of Si in solution is delayed by one day for the [VM50 + *P. putida*] experiment and by 4 days for the [VM25 + *P. putida*] experiment, compared to [VM100 + *P. putida*]. For P, we also observe a delay of the phenomenon of the decrease of the NLs which is related to the quantity of glass introduced in solution. The less glass there is, the later this phenomenon is observed.

A drop in Mn NLs is observed during the experiment for all biotic conditions (Fig. 5c, e, f). It occurs at different alteration times depending on the S/V ratio: after 2 days for [VM100 + *P. putida*], 3 days for [VM50 + *P. putida*] and 6 days for [VM25 + *P. putida*]. The results are similar for the two sets of experiments, however a small delay is observed for the second set of experiments concerning the chromatic variations and the Mn behavior. Therefore, for the altering conditions of VM glass with *P. putida*, only the NLs of the first set of experiments are reported for Mn. The comparison of the results of the first and second set of experiments is reported in Supplementary Fig. 4.

Initial dissolution rates

The calculated “initial dissolution rates” are reported in Table 1. In abiotic conditions, a good coefficient of determination ($R^2 > 0.99$) was obtained for the linear regression calculated with the data points from the first 3 days of experiments for the two glasses, with dissolution rate values of 1.5 and 1.9 g/m²/d respectively for [VNM100] and [VM100]. In biotic conditions, the Si curves show a less linear trend (R^2 between 0.8 and 0.95). The obtained dissolution rates are lower in biotic than in abiotic conditions, 0.9 g/m²/d for both [VNM100 + *P. putida*] and [VM100 + *P. putida*]. These values should be taken cautiously as they are calculated on the basis of dissolved Si measured in the filtered aliquots, without taking in account the biofilms, and acknowledging that several mechanisms can influence the presence of Si in the solution when bacteria are present.

Recovered bacteria mass

The results of the ICP-OES analysis of the mineralization of the recovered pellets and of the cleaning solutions are reported in Fig. 6 in wt% normalized to the weight of the dry pellet collected. The results obtained from the analysis of the mineralized recovered pellets represent the elements

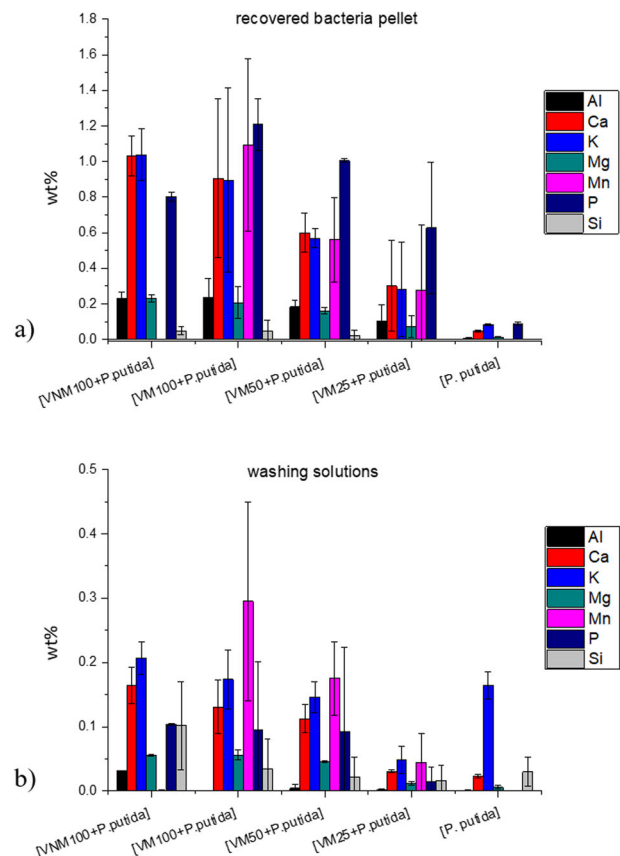


Fig. 6 Mass percentages. a Dry bacterial pellets, **b** Washing solutions recovered at the end of the experiments. Uncertainty bars correspond to the uncertainties calculated taking into account the analytical ICP-OES error (10%), and, when available, the standard deviation for the replicates.

incorporated within the bacteria. The results obtained from the analysis of the cleaning solutions represent the elements adsorbed on the surface of the cells.

Figure 6a represents the weight percentages of mineralized bacterial pellets for all the conditions tested. The bacterial pellets recovered from the experiments in presence of glass are enriched (up to 1.2 wt%) with all the elements dissolved from the glass (Al, Ca, K, Mg, Mn, P, Si). On the contrary, the bacterial pellet from [P. putida] presents only low mass percentages of Ca, K, and P (below 0.1 wt%). In general, for all conditions in the presence of VM glass, the elements that represent the highest weight percentages are Ca, K, Mn, and P, while Al, Mg, and Si represent very low weight fractions. The higher the S/V ratio, the more the bacterial pellet becomes enriched in elements from the glasses (weight percentages up to 1.2%, 1%, and 0.7% for the [VM100 + *P. putida*], [VM50 + *P. putida*] and [VM25 + *P. putida*] experiments, respectively). The ratio of elements remains the same, except for Mn. In fact, the weight percentages of Mn for [VM25 + *P. putida*] and [VM50 + *P. putida*] experiments are equivalent to those of Ca and K (ratio Mn/Ca and Mn/K between 0.92 and 1.00) and lower compared to P (ratio Mn/P between 0.44 and 0.56), while for the [VM100 + *P. putida*] experiment, Mn wt% is higher than Ca and K (Mn/Ca and Mn/K ratio of 1.21 and 1.22, respectively), and closer to P (Mn/P ratio = 0.9).

The washing solutions were analyzed by ICP-OES to estimate the amount of elements that were potentially adsorbed to the surface of the bacterial cells. The results in weight percentages are plotted in Fig. 6b. The weight percentages of elements in washing solutions are generally lower (between 0.1 and 0.3 wt%) than

those measured in the mineralization solutions (up to 1.4 wt%). The average Mn values for the [VM100] experiment has a high variability between the two replicates and a very high weight percentage value. It should be taken into account that i) in the altering solution recovered at the end of the experiment there may be residues of Mn-enriched biofilm in the form of floc, and ii) in the washing solution EDTA is a strong complexing agent. The Mn detected in the washing solution could therefore be the result of complexation of this element by EDTA not only on the surface of the bacterial cells but also on the surface of the biofilm suspended in solution. This said, for all the elements in the washing solutions of the VM weathering experiments, a relationship between the amount of elements detected and the S/V of the experiment is observed. The higher the S/V, the more elements are adsorbed. In particular, the average weight percentages for the [VM25 + *P. putida*] experiment are two or even three times lower than the values for the [VM50 + *P. putida*] and [VM100 + *P. putida*] experiments.

DISCUSSION

The results show that the presence of bacteria has an effect on the dissolution kinetics of the glass. Reciprocally, the glass amount and composition influence the bacterial growth and behavior. These two aspects will be discussed separately.

The altering solutions only contain sources of C and N as nutritive elements for the bacteria. The bacterial population introduced in the [*P. putida*] experiment is not able to grow on the only nutritive basis of the liquid medium (Fig. 2), and the population remains stable from the beginning to the end of the experiment. On the contrary, the bacterial population grows when glass is introduced in the altering solutions, both in presence of VM (planktonic bacterial suspension and biofilm formation) and VNM glass (only planktonic form observed) (Fig. 2). This result indicates that the elements released by the glass are necessary to the development of the bacterial cells. Some elements contained in the glass are known to be important macronutrients for microorganisms, such as K, Ca, Mg, P, while the role of Mn is still not totally understood. The presence of a biofilm in the culture containing VM might indicate that Mn acts as a modulator of biofilm production under environmental stress⁷⁰. If, in the present experimental setup, the bacterial cells are under stress (iron stress, oxidative stress), it seems that in the presence of VNM they are only able to respond to iron stress by producing the siderophore PVD^{43,45,66}, while in presence of VM they are also able to respond to oxidative stress in the form of biofilm production^{70,71}.

Regarding the bacterial growth, the OD results show a slightly lower bacterial growth for [VNM100 + *P. putida*] when compared to [VM100 + *P. putida*] (Fig. 2a). However, this difference is not significant within the experimental uncertainty, suggesting that bacterial growth is equivalent for both glasses and that Mn is not essential to the growth of the bacteria, which would be in agreement with the results from Jiang et al.⁷² who observed that the growth of *P. putida* MnB1 was not significantly influenced by Mn(II). Nevertheless, these results are only based on OD and CFU measurements obtained by sampling the culture surfactant liquid medium, thus only bacterial cells in planktonic form are considered. The biofilm produced during alteration experiments in the presence of VM is not taken into account by these methods. Therefore, only a quantification of the biomass in the biofilms would allow to decide on the significant effect of Mn on the development of bacteria, especially because biofilm formation is an important phenomenon for *P. putida*, so these results should be considered cautiously. OD measurements are generally only a proxy for biofilm development quantification, which could not be totally applied here since VM glass (and thus the presence of Mn) seems to favor the biofilm lifestyle while VNM glass without Mn favors the planktonic lifestyle.

Several studies^{35,43,54,56,61} have shown that bacterial growth for heterotrophic bacteria was more pronounced in the presence of a substrate containing Fe. Fe is a fundamental element as a cofactor of enzymes involved in several cellular enzymatic mechanisms essential to the life of bacteria. The nutritional value of Mn is less known and generally considered less important than that of Fe. Mn is a micronutrient that is also known for its role of cofactor for certain enzymatic mechanisms, but it is only involved in free radical detoxification mechanisms (response to oxidative stress) or in certain types of photo-synthesis as a cofactor⁷³. Mn oxidation by many bacterial strains has been documented^{26–28,65,67} but its physiological role remains poorly understood. A recent study by Yu and Leadbetter³⁰, showed that some bacterial strains exhibit exponential growth correlated to Mn oxidation, linked to a CO₂ fixation process. Manganese could in some cases participate in the carbon cycle and therefore in the energy cycle of certain bacteria. This discovery represents a turning point for the geomicrobiology of Mn and shows that the role of Mn in the life cycle of bacteria is still to be investigated.

In this work, a correlation was observed between the bacterial growth curves and the S/V ratio of the experiment (Fig. 2). It seems that bacterial growth is limited by the release of glass elements into solution. This confirms that the glass represents a source of nutrients for the bacteria. Notably, the results of the mineralization experiments of bacterial pellets recovered at the end of the VM biodissolution experiments show that the elements released by the glass have been scavenged by the bacterial cells. The presence of few amounts of Si in the recovered bacterial pellets could be explained by a “trapping” effect of the biofilm. This element has no nutritional value so its capture is probably a non-voluntary secondary effect.

After 8 days of experiment, the bacteria that grew in the [VM100 + *P. putida*] experiment are particularly enriched in P and Mn. The decrease, in solution, of Mn and P concomitantly with the appearance of the brown coloration suggests that the enrichment of P and Mn observed in the bacterial pellets after 8 days is related to the development of biofilm (rich in P) and the oxidation of Mn and its accumulation by the bacteria in the form of oxides in the glycocalyx, the extracellular organic matrix^{26,27,65,72}.

The proportions between the elements of the glass are different in the washing solution and the bacterial pellet. In the pellet, high amounts of P are found, while in the washing solutions higher amounts of K are detected. This confirms that P is a key element present in the glass for the development of bacteria, while the amount of K released from the glass is sufficient and in excess compared to what the bacteria need since it cumulated on the external surface of the cells. Moreover, the presence of P in solution is slightly different for the different S/V tested. The experiment with the higher S/V ratio [VM100 + *P. putida*], and characterized with the faster bacterial growth, is the one showing the lowest NLs of P in solution at the beginning of the experiment. The drop of P in solution happens later for the other experiments with lower S/V (after 6 days for VM50, and after 8 days for VM25). The uptake of P seems to concur with the beginning of the development of the bacterial population, confirming the key-role of P as a bacterial nutrient.

According to literature, the green hue observed in solution is attributed to siderophore production, while the brown color is attributed to Mn oxides formation^{26,64,65}. The results show that the bacteria start to produce pyoverdine when they are at a fairly advanced stage of development: for example, it is detected after 2 days in [VM100 + *P. putida*]. Moreover, no PVD production is observed for the [*P. putida*] experiment, the bacteria were not able to grow enough to produce the siderophore. PVD is detected in the presence of VNM and VM for all dissolution conditions tested, but with some differences concerning the time of production of PVD and its evolution in solution. In [VM100 + *P. putida*], PVD is produced since the beginning of the experiment; then, its

concentration decreases at the end of the experiment as the green coloration due to PVD is progressively replaced by a brown coloration. This latter is also related to the drop in Mn concentration in solution and the Mn-rich biofilm production. This is observed for all experiments in the presence of VM, with a time delay related to the amount of glass – and thus, of nutrients – introduced into solution. For the [VNM100 + *P. putida*] experiment, PVD concentration in solution reaches a plateau until the end of the experiment. A similar phenomenon was observed by Perez et al.⁴³ during biodissolution experiments of Fe-bearing and Fe-free glasses in presence of *Pseudomonas aeruginosa*, the typical PVD green color and absorption spectra were observed for Fe-bearing glasses only at the beginning of the dissolution tests, while for Fe-free glasses PVD was persistent in solution until the end of the experiments. This can be explained by the metabolic function of pyoverdines, which are generally produced under stress to promote the bioavailability of Fe, meaning that in presence of sufficient amounts of Fe released by the glass, PVD was not produced anymore because this element was already available. Thus, in the present work, PVD is released by *P. putida* because it is iron-starved and in order to enhance the availability of Fe; but in the absence of this element, Mn is alternatively complexed by the siderophore, triggering the whole Mn oxidation process. This does not mean, however, that Mn replaces Fe as a nutrient for this strain, in fact siderophore-mediated Mn uptake by microbes has not been demonstrated⁴⁸. To get more insight into what happens to PVD in solution, it is necessary to observe the evolution of the absorption spectra in the 300–500 nm region for the [VM100 + *P. putida*] experiment that lasted 13 days. The results show that the PVD in solution is present at first in its non-complexed form. The intensity of the corresponding absorption peak (peak B in Fig. 4b) increases with time, then starts to decrease after 3 days and a shift towards higher wavelengths, which indicates the formation of the complexed form PVD-Mn(III). This phenomenon is referred in the literature as pyoverdine fluorescence quenching because free PVD fluoresces, while the PVD-Mn complex does not. The formation of this complex was reported by Parker et al.^{64,65} in cultures of *P. putida* at pH 7.1–7.5. The stability constant of this complex is very high ($\log K = 47.5$), when both Fe and Mn coexist, Mn can compete with Fe ($\log K = 44.6$) for the complexation with PVD⁶⁴. The formation of the PVD-Mn(III) complex is coupled to a decrease in the absorbance of this peak at 410 nm and the appearance of a band at 335 nm, attributed to the degraded PVD (Fig. 4b). This phenomenon is associated with the decrease of Mn in solution and the appearance of the brown coloration due to the formation of Mn oxides. These observations are in agreement with the results of Parker et al.⁶⁵ that show that the complexation of Mn by PVD is one of the possible paths that lead to the oxidation of Mn. However, Parker et al.⁶⁵ argue that the presence of Mn does not cause the interruption of PVD production, whereas our results seem to show that PVD concentrations keeps decreasing (the band between 400 and 410 nm continues to lose intensity after 13 days) after the appearance of brown phases. Parker et al.⁶⁵ also observed the formation of the soluble PVD-Mn(III) complex. They then show the existence of a third pathway that goes through the degradation of the PVD-Mn(III) complex, the release of Mn(III) and the oxidation to MnO₂ by enzymatic way. This third scenario could likely explain the results of all the [VM + *P. putida*] experiments: the formation of the PVD-Mn(III) complex is observed by UV-VIS and is followed by the appearance of the band at 335 nm attributed to degraded PVD following the formation of Mn oxides. This mechanism has not yet been described in detail but it is generally attributed to an interaction between the complex and the CumA (multicopper-oxidase) enzyme, considered responsible for Mn oxidation, or to the interaction between the complex and the surface of the oxides already formed by the parallel enzymatic oxidation path⁶⁵. The apparent interruption of PVD production

seems to show that from a certain state of bacterial growth, direct MnO₂ formation is favored over PVD production. Another possibility is that after a certain growth phase, the process of PVD production and Mn oxidation slows down and almost stops, since the accumulation of Mn oxides in the extracellular matrix is known to happen mostly during the logarithmic or early stationary growth phase of the bacteria^{66,74}. The brown staining observed in optical microscopy in Fig. 3b is due to the accumulation of Mn oxides in the biofilm, which are found in the extracellular matrix surrounding the cells. These oxides have been extensively studied in the literature. Villalobos et al.^{26,67}, and Toner et al.⁷⁴, showed that birnessite type nanoparticles are formed, with an oxidation state of Mn between (III) and (IV) but closer to (IV). This microbial efficiency for the formation of oxides has led some authors to say that the majority of Mn oxides found in nature could be of biotic origin or derived from the alteration of these oxides²⁷.

According to the results of the [VM + *P. putida*] experiments, the following scenario can be hypothesized: Mn is released from the glass in solution, it is complexed by the PVD, which triggers the oxidation of Mn; after this phenomenon, the siderophore is found in its degraded form. The Mn oxides produced accumulate in the extracellular matrix composing the biofilm, which will adhere to the altered glass powder. Concerning the production of PVD, siderophores are generally produced by bacteria when iron-starved, in order to facilitate iron uptake^{37,43,75–77} and this is also true for *P. putida*^{64,66}. The physiological function of bacterial Mn oxidation remains unclear²⁸, consequently the connection between PVD production and Mn oxidation still has to be investigated. Future work will involve biodissolution experiments with *P. putida* and an Fe and Mn-bearing glass. This will help to elucidate the behavior of this bacterial strain in presence of these two elements, that generally have coupled biogeochemical cycles mediated by siderophores^{48,64}. In fact, as suggested in the literature^{48,64}, in natural environments Mn and Fe may compete for a limited pool of siderophores and have similar mineral dissolution pathways, meaning that there can be a competitive metal-siderophore complex formation during the dissolution of a Mn and Fe-bearing substrate.

A comparison between the two abiotic glass experiments, [VM100] and [VNM100], is first necessary to discuss the dissolution behavior of VM and VNM in the culture medium. In terms of NLs and dissolution rates, both glasses dissolve much faster in the culture medium used in the present work than in EUP solutions with 1 mM carbonate buffer used in a previous work⁶³. The dissolution rate of VM increases from 0.37 g/m²/d in EUP + carbonate buffer to 1.87 g/m²/d in sterile medium, and that of VNM increases from 0.88 to 1.50 g/m²/d (Table 1). The change in buffer can affect the dissolution kinetics. Moreover, the presence of other ions and compounds in the culture medium solution can also have additional effects on the dissolution behavior of glass (change of the ionic strength of the solution, change of pH, complexation effects). In particular, the glucose introduced in the culture medium as a carbon source for the bacteria could be responsible for an increase in the dissolution of glass, as it was demonstrated for feldspars in the presence of gluconates⁷⁸. VM dissolves faster than VNM in the sterile medium, which differs from the results obtained for the same glasses in EUP + carbonate buffer⁶³. Moreover, in this previous work, the addition of a siderophore in solution resulted in a greater increase in dissolution rate for VM glass than for VNM glass, suggesting that the complexation of Mn by the siderophore was a fundamental step in the glass dissolution process. The same reasoning could explain this difference in behavior of the two glasses in the culture medium. The VM shows here a higher dissolution rate than the VNM in the culture medium, which contrasts with what was observed in EUP. This could be attributed to the key role of Mn in the dissolution process: the Mn-bearing glass is more affected by

the presence of different compounds in solution possibly having chelating properties.

For both glasses, the NLs of Si in the presence of bacteria remain close to zero and increase after a few days of experiment. An immediate hypothesis would be that bacteria cause a slowing down of the hydrolysis of the glass. In the literature, contrasting observations have been reported regarding the catalyzing or, on the contrary, inhibiting effect of bacteria on the dissolution kinetics of minerals/glasses. In the study of Perez et al.⁴³ on the dissolution of basaltic glasses in the presence of *Pseudomonas aeruginosa*, an enhanced release of Si, Fe and Al was observed under biotic conditions compared to the abiotic controls. In this study, no biofilm was found on the surface of the glasses. Other authors^{78,79} evidenced that microbial attachment produces a microenvironment on mineral surface that accelerates the dissolution of silicates, particularly by releasing elements such as P and Fe. Biofilms are generally considered to accelerate dissolution through water retention and localized exudate production³⁸. Indeed, within a biofilm it is possible to find gradients of element concentration or gradients of pH and redox potential³⁵. In the work of Stockmann et al.⁶² on the dissolution of basaltic glass in the presence of *Pseudomonas reactans*, lower Si dissolution rates were observed in continuous reactors containing dead or living bacterial cells. Shirokova et al.⁵⁵ observed a negligible effect of *P. reactans* on olivine dissolution, and a recent study⁵⁷ showed that *P. reactans* had a weak impact on the dissolution of Ca and Mg bearing silicates. Other studies have also shown the dissolution-inhibiting effect of biofilm attachment and its ability to retain most elements present in the system^{61,80,81}. These differences in behavior show how much the weathering properties vary from species to species (even within the same genus *Pseudomonas*) and from one substrate to another, and suggests that the importance of biofilm in biodissolution experiments is often underestimated. The mineralization results of the recovered bacteria pellets show that valued information is retained in the biofilm and that the analysis of the leaching solutions only gives a partial information of what happens.

A link between the delayed “apparent” release of Si and the production of PVD can also be found. The time at which the Si NLs start to rise generally corresponds to the time of PVD production. The presence of PVD seems to act as a catalyst of the dissolution of the glass. Siderophores have been shown in several studies and notably in a previous work with the same glass samples to increase the dissolution rates of the glasses, through complexation reaction between siderophore molecules and Mn from the glass, leading to the destabilization of the silicate network and accelerating its hydrolysis⁶³. The fall in Mn NLs (PWD production, Mn consumption and Mn oxides formation) coincides with the rise in the Si NLs. One hypothesis could thus be that the increase in Si “apparent” release in the bacterial medium would be due to acceleration of the hydrolysis rate of the glass as a result of PVD-Mn complex formation and Mn consumption into secondary phases.

The fact that the stoichiometry of other elements such as K, Ca, P remains unchanged at the beginning of the dissolution experiments in the presence of bacteria can make this scenario favorable: Si is released in solution with the other elements, then “trapped” on the surface of the cells. In this case, the Si would be immediately “trapped”, which is consistent with the results of the bacterial pellet analysis. This last option is therefore the most likely. However, Si is not known to be used in cellular metabolisms and it is therefore an unintended side effect.

Regarding K, a change in the stoichiometry of K dissolution for both conditions of VM dissolution at low S/V ratios is observed. Indeed, in [VM50 + *P. putida*] and [VM25 + *P. putida*], the NLs of K are significantly higher than the other elements, when compared to its behavior in the [VM 100 + *P. putida*] experiment. The pH measurements reported in Table 1 show that the presence of

bacteria acidifies the solution (production of acids or protons) particularly in the presence of the smallest S/V. This could intensify the interdiffusion mechanism, as observed in the presence of organic acid⁶³. We have seen that the experiments with lower S/V values [VM50 + *P. putida*] and [VM25 + *P. putida*] show a delay with respect to the [VM100 + *P. putida*] experiment concerning all the parameters taken into account (bacterial growth, PVD production, effect on the stoichiometry of Mn and P). This means that they can be used as a way to observe in more detail the phenomena happening at the beginning of the biodissolution, which happen too rapidly to be observed in the [VM100 + *P. putida*] experiment. The observation of a significant decrease in pH coupled to an increase of K NLs for the experiments [VM50 + *P. putida*] and [VM25 + *P. putida*] could be a sign that at first, the bacteria produce acid species (H⁺, inorganic or organic acids) that cause the acidification of the solution. This acidification of the solution by the bacteria promotes the interdiffusion mechanisms that causes a preferential release of K. This ion-exchange is responsible for the pH rise observed in the other experimental conditions, but it seems that at the beginning of the experiment, an excess of acid is produced, or that the acids production is faster than ion-exchange. In fact, it appears that in the first moments of the bioalteration experiments, the ion-exchange still has not counter-balanced the fall of pH caused by the acids, that is why we observe at the same time a lower pH and a stronger release of K.

Then, when the bacteria growth is more advanced because of the uptake of nutritive elements released by the glass, the acids production slows down or stops, while the PVD production starts, and consequently Mn oxidation. The initial production of acid species followed by the production of siderophores could also be in agreement with the hypothesis that organic acids (with chelating properties) can also have a role of promoting the release of metallic cations from the surface, transporting them as aqueous complexes to be later scavenged by aqueous siderophores^{36,40}. This synergistic effect of organic acids and siderophores was not observed in a previous work on the dissolution of the same model glass in presence of oxalic acid and the siderophore DFOB⁶³. However, it has to be taken into account that a simplified system in a laboratory experiment cannot exactly mimic the complex biologically produced mechanisms; for example, the rate of production of acid molecules and siderophores and relative concentrations of these molecules in solution at different times of the biotic experiment could generate a different outlook. Moreover, an important difference could be the nature of the acid species (not identified in this work) and the kind of siderophore used; DFOB is a trihydroxamate siderophore, while PVD is a mixed-moietry siderophore with hydroxamate, catecholate and α -hydroxycarboxylate groups^{47,66}.

These results allow to elucidate the behavior of the bacteria in presence of glass and in need of nutrients. It seems that the production of acids is the first “weapon” they use to change the environment in order to facilitate the uptake of nutrients, while the production of siderophore only intervene in a second moment, when they have already sufficiently grown.

The appearance of the browning phenomenon on medieval stained-glass windows is linked to the presence of an internal or external source of Mn and to the capacity of this element to form brown oxidized phase inside the altered layer of glass. The results described above, together with the results described in Valbi et al.⁶³ allow us to clarify the possible mechanisms for the appearance of browning on stained glass windows. Several paths can be identified by dissecting the phenomenon: the Mn solubilization step and the brown phase formation step. Both steps can occur via an abiotic pathway or a biotic pathway. Regarding the solubilization step, we have seen that Mn is abiotically released by the glass in UPW solution and in a sterile culture medium (bacteria-free). This is in agreement with the literature data which show the weathered layer

Table 2. Composition (in oxide weight %) obtained by microprobe analysis of the two synthesized glasses.

Wt %	SiO ₂	Al ₂ O ₃	P ₂ O ₅	Na ₂ O	CaO	MgO	K ₂ O	MnO	Total
Mn-bearing glass (VM)	51.5 ± 0.4	1.8 ± 0.0	3.2 ± 0.2	1.2 ± 0.0	17.3 ± 0.2	4.3 ± 0.1	18.3 ± 0.1	2.0 ± 0.1	99.8 ± 0.3
Mn-free glass (VNM)	52.4 ± 0.5	1.9 ± 0.1	3.4 ± 0.3	1.2 ± 0.0	17.6 ± 0.2	4.3 ± 0.1	18.8 ± 0.3	0.0 ± 0.1	99.7 ± 0.4

Standard deviations are calculated on 10 measurements performed on each sample.

around the brown phases is depleted in Mn compared to the pristine glass. Mn can also be released biotically indirectly by complexation with exudates produced by microorganisms. The interaction with these exudates in diluted conditions can cause a higher dissolution rate of the glass and thus an increase of the concentration of the glass elements in solution. For the brown phase formation step, the present work showed that the Mn oxides produced by *P. putida* are located inside the biofilm formed on the surface of the altered glass. The characterization of historical stained-glass^{19–21} shows that the brown spots are located inside the altered layer. This might be interpreted as a sign that bacteria are most likely not involved in the second step of the appearance of the browning phenomenon. However, although the morphology of this biotic brown phase is different from the one observed on the stained glass, we have seen that the presence of *P. putida* has a strong effect on the evolution of Mn and P in solution. This is worth noticing since the brown phase found on some stained glasses from the work of Ferrand et al.²⁰ shows chemical and structural correspondences with purpurite, a Mn phosphate. It is therefore not possible to exclude a bacterial implication in the formation of these Mn and P-bearing brown phases. Moreover, the results of 8-days experiments cannot be directly compared with an alteration phenomenon which probably happens on a much longer time scale; thus, it has to be taken into account the effect of time on the becoming of these brown phases produced by the bacteria, long-time experiments should be conducted in order to evaluate the evolution of these brown phases in different conditions. The non-homogeneous distribution of bacteria and the high diversity of strains depending on the localization of the panel, the internal/external faces^{33,82,83} on the surface of the glass could also explain the appearance of the browning phenomenon in localized spots in the altered glass.

In conclusion, the present work evidenced several correlations between the growth and the behavior of a specific Mn-oxidizer strain and the presence, nature and the amount of glass the bacteria are in contact with. The higher the surface/volume (S/V) ratio of the experiment, the faster the bacterial growth. The S/V in the bacterial medium is also correlated with the quantity of pyoverdine produced by the cells and the formation of Mn oxides. These different behaviors have reciprocally an effect on release of elements induced by the dissolution of the glass, showing that the dissolution mechanisms of a glass in direct contact with a siderophore producing-bacteria are more complex than those evidenced by abiotic studies implying siderophores. More in general, it was shown that at the beginning of the dissolution process the presence of bacteria increases the dissolution of glass by the production of acid species that favor the interdiffusion mechanism, while the siderophore production starts at an advanced stage of bacterial growth. The presence of *P. putida* and the production of the PVD siderophore did not seem to increase the rate of glass dissolution, but an important role of both bacterial cells and biofilm was highlighted as sink for dissolved elements, especially Mn, P (used for the bacterial metabolism) and Si (trapped within the biofilms). Detailed information on the uptake of nutritive elements by the microorganisms at different moments of their development were obtained, and brown phases were biotically produced by bacteria starting from Mn present in the glass. The direct implication of the bacteria in the appearance

of the browning phenomenon cannot still be confirmed though, since more long-term experiments should be conducted to investigate the evolution of these brown phases with time.

METHODS

Glass samples

The composition of the potash-lime-silica model glasses (Table 2) is representative of medieval stained-glass windows^{8,9,20,84}. Two compositions were chosen: a Mn-bearing glass (VM) and a Mn-free glass (VNM). Although present in most medieval compositions, Fe was not introduced in the glass in order to only focus on Mn since these two elements can be involved in similar chemical or biochemical mechanisms⁴⁸. Model glasses were prepared with a procedure described elsewhere⁶³. The composition of the obtained glass was checked by microprobe analysis on a Cameca SX Five instrument (Table 2). Samples were embedded in resin, polished and carbon-coated. A tension of 15 kV was used for the analysis, with a current of 4 nA. Silicate minerals were used as calibration standards. The glass was then grounded and sieved in order to collect the 100–200 µm powder size fractions. This powder fraction was cleaned by sedimentation in acetone to remove residual fine particles. The homogeneous size distribution was checked with a table scanning electron microscopy TM3030 in backscattered electrons mode at 15 kV. BET measurements were performed by krypton adsorption in order to estimate the specific surface area of the samples. Different batches of powder were prepared following the same procedure and the average reactive surface area is 0.028 ± 0.002 m²/g. According to the literature, the Mn-bearing glass probably contains a mixture of Mn(II) and Mn(III)^{13,85–87}.

Biodissolution experiments

The altering solutions were prepared from Ultra Pure Water (UPW). The HEPES buffer was introduced in order to stabilize the pH, it belongs to the Good's family of buffers⁸⁸ and is often used in biochemical experiments. This buffer is impermeable to biological membranes, is supposed to have low chelating properties towards metallic cations, is not toxic and does not take part in biochemical reactions⁵². Only C and N were introduced in the altering solutions as nutritive elements for the bacteria, since they are not available in the glass. The final composition of the altering solutions (adapted from Perez et al.⁴³) is: glucose 1 g/l, NH₄Cl 1 g/l, NaCl 0.5 g/l, HEPES buffer 10 mM, pH 6.5. An initial culture of *Pseudomonas Putida* MnB1 strain (ATC23483) grown in Lisogen Broth (LB) medium (peptone 10 g/l, yeast extract 5 g/l, NaCl 5 g/l) was kept at 5 °C. At the beginning of each dissolution experiment, 1 ml of this solution was used to inoculate 200 ml of fresh LB medium. The bacteria were left to grow in this fresh LB medium at 25 °C and 160 rpm for around 24 hours. Then, once the medium had a OD between 1.0 and 1.2 (unitless), 1 ml aliquots of this new LB medium were used to inoculate the altering solutions for the dissolution experiments in the presence of bacteria. A blank sample was systematically collected before the introduction of the glass. After the blank sampling, the glass powder (with a size distribution between 100–200 µm) was immersed in 200 ml of solution into pyrex Erlenmeyers of 500 ml, previously washed in a nitric acid bath and washed three times with UPW. The eventual

contribution of the pyrex glass is not taken into account as the dissolution rates of pyrex glass are of several orders of magnitude lower than for a potash-lime-silicate glass and thus negligible. Moreover, no chemical pollution from the pyrex glass was observed in the blank samples nor in the control conditions without glass samples. The Erlenmeyers containing the medium were autoclaved before addition of the microorganisms and of the glass. The glass powders were sterilized by UV-light exposure for 30 min directly in the sterile environment where the preparation of the experiments was carried on. No microbial contamination by other organisms was observed throughout the whole experiments. Different Surface/Volume (S/V) ratios were investigated for the VM glass by introducing 100 mg [VM100 + *P. putida*], 50 mg [VM50 + *P. putida*] or 25 mg [VM25 + *P. putida*] of glass into constant volume of solution (200 ml). Only the 100 mg experiment was tested for the VNM glass [VNM100 + *P. putida*]. Abiotic conditions were realized as well, [VM100] and [VNM100] conditions containing the glass in the altering solution without the bacteria. A biotic condition without glass, only containing the bacteria in the altering solution [*P. putida*], was also carried out (Fig. 1). The suspensions were continuously shaken at 160 rpm (chosen to avoid mechanical damage and ensure the preservation of biofilm structures) at a controlled temperature of 25 °C for 8 days in a dark environment. Solution samples were collected during the dissolution experiment at time 0, 6 hours, 1, 2, 3, 6, and 8 days. One additional experiment was extended until 13 days with additional samplings. Each sampling was performed by removing 3 ml aliquots using a 5 ml syringe and filtered with 0.2 µm cellulose-acetate syringe filters. The total amount of sampled solution corresponds to less than 10% of the total starting volume, to ensure limited variations of S/V. The pH was measured at the beginning and at the end of the experiments with an Ag/AgCl type electrode. In order to perform ICP-OES analysis, the collected samples and the calibrating solutions were acidified to 5% (vol.) with HNO₃. The leachates were analyzed with a Perkin Elmer Optima 8300 ICP-OES to determine the concentrations of dissolved Si, Al, Mg, Ca, Mn, K, P. ICP calibration solutions were prepared by dissolving silicon and multielement commercial solution (Merck Chemicals) in UPW. Analytical absolute errors on elemental concentrations were determined for each element by analyzing several times the calibrating solutions. The analytical errors were calculated for each range of concentration for each element by evaluating the accuracy of the measurement over the average of 10 measurements. The percentage error is generally between 1 and 10% for all elements in all concentration ranges evaluated, except for Si and K concentrations lower than 100 ppb where the error is 10 to 50%. From the concentration values, the normalized mass loss $NL_{(i)}$ (Eq. 1) for each element *i* of each leachate sample is calculated in order to normalize the results to the amount of the concerned element within the glass composition and to the S/V ratio.

$$NL_{(i)} = \frac{c_i}{S/V \times x_i} \quad (1)$$

c_i is the concentration of the element *i* in solution, S is the surface of glass exposed to the solution and V is the volume of the solution. x_i is the mass fraction of the element *i* in the glass. Initial rate of dissolution $r_{(i)}$ (Eq. 2) was determined by plotting the $NL_{(i)}$ versus time and adjusting a linear regression on the initial slope of the curve. Generally, 4 to 6 points were chosen by picking the maximum number of linear points for each fit.

$$r_{(i)} = \frac{dNL_{(i)}}{dt} \quad (2)$$

The absolute error on the $NL_{(i)}$ was calculated using the propagation of uncertainty law, taking into account the analytical ICP-OES error (10%), the uncertainty on the measurement of reactive surface area (8%), and the experimental uncertainty $\pm SD$

for the two experimental replicates varying for each point, while the error on V and x_i are assumed to be negligible. All the experiments were repeated twice.

Recovery and analysis of bacterial pellets and washing solutions

At the end of the experiment, the altering solutions were collected and centrifuged paying attention to not recover the glass powders. The solutions were centrifuged 1 h at 4500 rpm. The supernatant was thrown away and the bacterial pellet was resuspended in a washing solution (EDTA 2 mM, BisTris 20 mM, pH 8). These solutions were centrifuged 20 minutes at 4500 rpm, 3 ml of supernatant were sampled, filtered and acidified for ICP-OES analysis. The bacterial pellet was collected and left to dry at 50 °C overnight. The dry pellet was then dissolved in 10 ml of HNO₃ 65% and warmed up to 90 °C until reduction of the solution to 2 ml (mineralization process). The final volume was completed to 20 ml with UPW and the resulting solution was analyzed by ICP-OES analysis.

OM and SEM observations

The altered glass powders were recovered at the end of the experiment and observed by Optical Microscopy with a KEYENCE VHX6000 numerical microscope and then with a table scanning electron microscopy equipped with an Energy Dispersive X-rays detector (SEM-EDX) TM3030. The altered glass powders were observed in environmental conditions of low vacuum with neither sample preparation nor coating and backscattered electrons images were obtained at 15 kV.

Bacterial growth and siderophore detection

For each sampling, 1 ml of non-filtered solution were dedicated to monitor the growth curves for *P. putida* by Optical Density (OD) measurements at 600 nm using a UV-1800 Shimadzu UV-VIS spectrophotometer and by plate counting Colony-Forming Unit (CFU). Dilutions of the sampled bacterial medium were plated on LB agar and incubated 24 h at 25 °C for the counting step. OD measurements were plotted versus CFU measurements and R^2 values were calculated by linear regression in order to check the accordance of the two methods.

Filtered leachates (cellulose acetate filters, Ø0.2 µm) were also analyzed in the same spectrophotometer at 402 nm in order to follow the production of the siderophore pyoverdine (PVD) during the dissolution experiment⁶⁵ as a function of time. The evolution of the absorption spectrum of PVD was also monitored by acquisition of the whole absorption spectrum between 300 and 500 nm for the supplementary experiment that lasted 13 days. Identical spectrophotometric cells were used for all measurements, with a standard optical path length.

DATA AVAILABILITY

The research data, consisting of the raw results from the dissolution experiments are available in the EarthChem Database [<https://doi.org/10.26022/IEDA/112513>].

Received: 31 August 2022; Accepted: 6 March 2023;

Published online: 29 March 2023

REFERENCES

- Shortland, A., Schachner, L., Freestone, I. & Tite, M. Natron as a flux in the early vitreous materials industry: sources, beginnings and reasons for decline. *J. Archaeol. Sci.* **33**, 521–530 (2006).
- Verità, M. Modern and ancient glass: Nature, composition and deterioration mechanisms. *Mater. Cult. Herit. Their Environ.* 119–132 (2006).
- Sterpenich, J. & Libourel, G. Using stained glass windows to understand the durability of toxic waste matrices. *Chem. Geol.* **174**, 181–193 (2001).

4. Gentaz, L., Lombardo, T., Loisel, C., Chabas, A. & Vallotto, M. Early stage of weathering of medieval-like potash-lime model glass: Evaluation of key factors. *Environ. Sci. Pollut. Res.* **18**, 291–300 (2011).

5. Lombardo, T. et al. Characterisation of complex alteration layers in medieval glasses. *Corros. Sci.* **72**, 10–19 (2013).

6. De Ferri, L., Lottici, P. P. & Vezzalini, G. Characterization of alteration phases on Potash-Lime-Silica glass. *Corros. Sci.* **80**, 434–441 (2014).

7. Verney-Carron, A. et al. Understanding the mechanisms of Si-K-Ca glass alteration using silicon isotopes. *Geochim. Cosmochim. Acta* **203**, 404–421 (2017).

8. Sessegolo, L. et al. Long-term weathering rate of stained-glass windows using H and O isotopes. *Npj Mater. Degrad.* **2**, 17 (2018).

9. Sessegolo, L. et al. Alteration rate of medieval potash-lime silicate glass as a function of pH and temperature: A low pH-dependent dissolution. *Chem. Geol.* **550**, 119704 (2020).

10. Mirti, P., Davit, P. & Gulmini, M. Colourants and opacifiers in seventh and eighth century glass investigated by spectroscopic techniques. *Anal. Bioanal. Chem.* **372**, 221–229 (2002).

11. Quartieri, S., Triscari, M., Sabatino, G., Boscherini, F. & Sani, A. Fe and Mn K-edge XANES study of ancient Roman glasses. *Eur. J. Mineral.* **14**, 749–756 (2002).

12. Jackson, C. M. Making colourless glass in the Roman period. *Archaeometry* **47**, 763–780 (2005).

13. Arletti, R., Quartieri, S. & Freestone, I. C. A XANES study of chromophores in archaeological glass. *Appl. Phys. A* **111**, 99–108 (2012).

14. Gliozzo, E. The composition of colourless glass: A review. *Archaeol. Anthropol. Sci.* **9**, 455–483 (2016).

15. Rossano, S. et al. Glass colourations caused by Mn-Fe redox pair: Application to ancient glass technology. *J. Non-Cryst. Solids* **594**, 121710 (2022).

16. Pilz, M. Traitements de conservation pour les vitraux altérés et brunis. *Programme Fr.-Allem. Rech. Pour Conserv. Monum. Hist.* 1995–1996 330–346 (1997).

17. Weber, L. G., Eggert, G. & Watkinson, D. A Closer Look at Brown Staining on Archaeological Glass. *Glass Ceram. Conserv. 2007 Interim Meet. ICOM-CC Work. Group* 35–45 (2007).

18. Gulmini, M., Pace, M., Ivaldi, G., Ponzi, M. N. & Mirti, P. Morphological and chemical characterization of weathering products on buried Sasanian glass from central Iraq. *J. Non-Cryst. Solids* **355**, 1613–1621 (2009).

19. Schalm, O. et al. Manganese staining of archaeological glass: The characterization of mn-rich inclusions in leached layers and a hypothesis of its formation. *Archaeometry* **53**, 103–122 (2011).

20. Ferrand, J. et al. Browning Phenomenon of Medieval Stained Glass Windows. *Anal. Chem.* **87**, 3662–3669 (2015).

21. Nyuys, G., Cagno, S., Bugani, S. & Janssens, K. Micro-XANES study on Mn browning: Use of quantitative valence state maps. *J. Anal. Spectrom.* **30**, 642–650 (2015).

22. Perez y Jorba, M., Dallas, J. P., Bauer, C., Bahezre, C. & Martin, J. C. Deterioration of stained glass by atmospheric corrosion and micro-organisms. *J. Mater. Sci.* **15**, 1640–1647 (1980).

23. Krumbein, W. E., Urzi, C. E. & Gehrmann, C. Biocorrosion and Biodeterioration of Antique and Medieval Glass. *Geomicrobiol. J.* **9**, 139–160 (1991).

24. Drewello, R. & Weissmann, R. Microbially influenced corrosion of glass. *Appl. Microbiol. Biotechnol.* **47**, 337–346 (1997).

25. Orial, G., Warscheid, T., Bousta, F. & Loisel, C. Incidence bactérienne dans les phénomènes de brunissement des vitraux anciens TT - Microbial impact in the browning of old stained glass windows. *Actual. Chim.* **312–313**, 34–39 (2007).

26. Villalobos, M., Toner, B., Bargar, J. & Sposito, G. Characterization of the manganese oxide produced by *Pseudomonas putida* strain MnB1. *Geochim. Cosmochim. Acta* **67**, 2649–2662 (2003).

27. Tebo, B. M. et al. Biogenic manganese oxides: Properties and mechanisms of formation. *Annu. Rev. Earth Planet. Sci.* **32**, 287–328 (2004).

28. Tebo, B. M., Johnson, H. A., McCarthy, J. K. & Templeton, A. S. Geomicrobiology of manganese(II) oxidation. *Trends Microbiol.* **13**, 421–428 (2005).

29. Webb, S. M., Dick, G. J., Bargar, J. R. & Tebo, B. M. Evidence for the presence of Mn(III) intermediates in the bacterial oxidation of Mn(II). *Proc. Natl. Acad. Sci.* **102**, 5558–5563 (2005).

30. Yu, H. & Leadbetter, J. R. Bacterial chemolithoautotrophy via manganese oxidation. *Nature* **583**, 453–458 (2020).

31. Gorbushina, A. A. & Palinska, K. A. Biodeteriorative processes on glass: experimental proof of the role of fungi and cyanobacteria. *Aerobiologia* **15**, 183–191 (1999).

32. Carmona, N. et al. Biodeterioration of historic stained glasses from the Cartuja de Miraflores (Spain). *Int. Biodeterior. Biodegrad.* **58**, 155–161 (2006).

33. Piñar, G. et al. Microscopic, chemical, and molecular-biological investigation of the decayed medieval stained window glasses of two Catalonian churches. *Int. Biodeterior. Biodegrad.* **84**, 388–400 (2013).

34. Drever, J. I. & Stillings, L. L. The role of organic acids in mineral weathering. *Colloids Surf. Physicochem. Eng. Asp.* **120**, 167–181 (1997).

35. Liermann, L. J., Barnes, A. S., Kalinowski, B. E., Zhou, X. & Brantley, S. L. Micro-environments of pH in biofilms grown on dissolving silicate surfaces. *Chem. Geol.* **171**, 1–16 (2000).

36. Cheah, S. F., Kraemer, S. M., Cervini-Silva, J. & Sposito, G. Steady-state dissolution kinetics of goethite in the presence of desferrioxamine B and oxalate ligands: Implications for the microbial acquisition of iron. *Chem. Geol.* **198**, 63–75 (2003).

37. Kraemer, S. M. Iron oxide dissolution and solubility in the presence of siderophores. *Aquat. Sci.* **66**, 3–18 (2004).

38. Brehm, U., Gorbushina, A. & Mottershead, D. The role of microorganisms and biofilms in the breakdown and dissolution of quartz and glass. *Palaeogeogr. Palaeoclimatol. Palaeoecol.* **219**, 117–129 (2005).

39. Cama, J. & Ganor, J. The effects of organic acids on the dissolution of silicate minerals: A case study of oxalate catalysis of kaolinite dissolution. *Geochim. Cosmochim. Acta* **70**, 2191–2209 (2006).

40. Reichard, P. U., Kretzschmar, R. & Kraemer, S. M. Dissolution mechanisms of goethite in the presence of siderophores and organic acids. *Geochim. Cosmochim. Acta* **71**, 5635–5650 (2007).

41. Peña, J., Duckworth, O. W., Bargar, J. R. & Sposito, G. Dissolution of hausmannite (Mn3O4) in the presence of the trihydroxamate siderophore desferrioxamine B. *Geochim. Cosmochim. Acta* **71**, 5661–5671 (2007).

42. Perez, A. et al. Impact of iron chelators on short-term dissolution of basaltic glass. *Geochim. Cosmochim. Acta* **162**, 83–98 (2015).

43. Perez, A. et al. Bioalteration of synthetic Fe(III)-, Fe(II)-bearing basaltic glasses and Fe-free glass in the presence of the heterotrophic bacteria strain *Pseudomonas aeruginosa*: Impact of siderophores. *Geochim. Cosmochim. Acta* **188**, 147–162 (2016).

44. Fischer, T. B., Heaney, P. J. & Post, J. E. Changes in the structure of birnessite during siderophore-promoted dissolution: A time-resolved synchrotron X-ray diffraction study. *Chem. Geol.* **476**, 46–58 (2018).

45. Perez, A. et al. Direct and indirect impact of the bacterial strain *Pseudomonas aeruginosa* on the dissolution of synthetic Fe(III)- and Fe(II)-bearing basaltic glasses. *Chem. Geol.* **523**, 9–18 (2019).

46. Ahmed, E. & Holmström, S. J. M. Microbe–mineral interactions: The impact of surface attachment on mineral weathering and element selectivity by micro-organisms. *Chem. Geol.* **403**, 13–23 (2015).

47. Boukhalfa, H., Reilly, S. D., Michalczyk, R., Iyer, S. & Neu, M. P. Iron(III) Coordination Properties of a Pyoverdin Siderophore Produced by *Pseudomonas putida* ATCC 33015. *Inorg. Chem.* **45**, 5607–5616 (2006).

48. Duckworth, O. W., Bargar, J. R. & Sposito, G. Coupled biogeochemical cycling of iron and manganese as mediated by microbial siderophores. *BioMetals* **22**, 605–613 (2009).

49. Duckworth, O. W., Akafia, M. M., Andrews, M. Y. & Bargar, J. R. Siderophore-promoted dissolution of chromium from hydroxide minerals. *Environ. Sci. Process. Impacts* **16**, 1348–1359 (2014).

50. Akafia, M. M., Harrington, J. M., Bargar, J. R. & Duckworth, O. W. Metal oxyhydroxide dissolution as promoted by structurally diverse siderophores and oxalate. *Geochim. Cosmochim. Acta* **141**, 258–269 (2014).

51. Kalinowski, B. E., Liermann, L. J., Brantley, S. L., Barnes, A. & Pantano, C. G. X-ray photoelectron evidence for bacteria-enhanced dissolution of hornblende. *Geochim. Cosmochim. Acta* **64**, 1331–1343 (2000).

52. Kalinowski, B. E., Liermann, L. J., Givens, S. & Brantley, S. L. Rates of bacteria-promoted solubilization of Fe from minerals: a review of problems and approaches. *Chem. Geol.* **169**, 357–370 (2000).

53. Liermann, L. J., Kalinowski, B. E., Brantley, S. L. & Ferry, J. G. Role of bacterial siderophores in dissolution of hornblende. *Geochim. Cosmochim. Acta* **64**, 587–602 (2000).

54. Maurice, P. A. & Vie, M. A. Enhancement of Kaolinite Dissolution by an Aerobic *Pseudomonas mendocina* Bacterium. *Geomicrobiol. J.* **18**, 21–35 (2001).

55. Shirokova, L. S. et al. Effect of the heterotrophic bacterium *Pseudomonas* reactans on olivine dissolution kinetics and implications for CO2 storage in basalts. *Geochim. Cosmochim. Acta* **80**, 30–50 (2012).

56. Ferret, C. et al. Siderophore-promoted dissolution of smectite by fluorescent *Pseudomonas*. *Environ. Microbiol. Rep.* **6**, 459–467 (2014).

57. Pokrovsky, O. S., Shirokova, L. S., Zabelina, S. A., Jordan, G. & Bénédith, P. Weak impact of microorganisms on Ca, Mg-bearing silicate weathering. *Npj Mater. Degrad.* **5**, 51 (2021).

58. Rodrigues, A., Fearn, S., Palomar, T. & Vilarigues, M. Early stages of surface alteration of soda-rich-silicate glasses in the museum environment. *Corros. Sci.* **143**, 362–375 (2018).

59. Staudigel, H., Chastain, R. A., Yayanos, A. & Bourcier, W. Biologically mediated dissolution of glass. *Chem. Geol.* **126**, 147–154 (1995).

60. Gallien, J.-P., Gouget, B., Carrot, F., Eve Orial, G. & Brunet, A. Alteration of glasses by micro-organisms. *Nucl. Instrum. Methods Phys. Res. Sect. B Beam Interact. Mater.* **181**, 610–615 (2001).

61. Aouad, G., Crovisier, J. L., Geoffroy, V. A., Meyer, J. M. & Stille, P. Microbially-mediated glass dissolution and sorption of metals by *Pseudomonas aeruginosa* cells and biofilm. *J. Hazard. Mater.* **136**, 889–895 (2006).
62. Stockmann, G. J. et al. Does the presence of heterotrophic bacterium *Pseudomonas reactans* affect basaltic glass dissolution rates? *Chem. Geol.* **296–297**, 1–18 (2012).
63. Valbi, V. et al. Impact of biogenic exudates on the dissolution and browning of stained glass windows. *Int. Biodegradation. Biodegrad.* **173**, 105442 (2022).
64. Parker, D. L., Sposito, G. & Tebo, B. M. Manganese(III) binding to a pyoverdine siderophore produced by a manganese(II)-oxidizing bacterium. *Geochim. Cosmochim. Acta* **68**, 4809–4820 (2004).
65. Parker, D. L. et al. Inter-relationships of MnO₂ precipitation, siderophore–Mn(III) complex formation, siderophore degradation, and iron limitation in Mn(II)-oxidizing bacterial cultures. *Geochim. Cosmochim. Acta* **71**, 5672–5683 (2007).
66. Parker, D. L. et al. Pyoverdine synthesis by the Mn(II)-oxidizing bacterium *Pseudomonas putida* GB-1. *Front. Microbiol.* **5**, 202 (2014).
67. Villalobos, M., Lanson, B., Manceau, A., Toner, B. & Sposito, G. Structural model for the biogenic Mn oxide produced by *Pseudomonas putida*. *Am. Mineral.* **91**, 489–502 (2006).
68. Doremus, R. H. Interdiffusion of hydrogen and alkali ions in a glass surface. *J. Non-Cryst. Solids* **19**, 137–144 (1975).
69. Cailleteau, C. et al. Insight into silicate-glass corrosion mechanisms. *Nat. Mater.* **7**, 978–983 (2008).
70. Zheng, Y. et al. *bifA* regulates biofilm development of *Pseudomonas putida* MnB1 as a Primary Response to H₂O₂ and Mn²⁺. *Front. Microbiol.* **9**, 1490 (2018).
71. Gjermansen, M., Ragas, P. & Tolker-Nielsen, T. Proteins with GGDEF and EAL domains regulate *Pseudomonas putida* biofilm formation and dispersal. *FEMS Microbiol. Lett.* **265**, 215–224 (2006).
72. Jiang, S., Kim, D.-G., Kim, J.-H. & Ko, S.-O. Characterization of the biogenic manganese oxides produced by *Pseudomonas putida* strain MnB1. *Environ. Eng. Res.* **15**, 183–190 (2010).
73. Kehres, D. G. & Maguire, M. E. Emerging themes in manganese transport, biochemistry and pathogenesis in bacteria. *FEMS Microbiol. Rev.* **27**, 263–290 (2003).
74. Toner, B., Fakra, S., Villalobos, M., Warwick, T. & Sposito, G. Spatially resolved characterization of biogenic manganese oxide production within a bacterial biofilm. *Appl. Environ. Microbiol.* **71**, 1300–1310 (2005).
75. Stintzi, A., Dhungana, S. & Crumbliss, A. L. Microbial iron transport via a siderophore shuttle: A membrane ion transport paradigm. *Chemtracts* **14**, 258–265 (2001).
76. Saha, R., Saha, N., Donofrio, R. S. & Bestervelt, L. L. Microbial siderophores: A mini review. *J. Basic Microbiol.* **53**, 303–317 (2012).
77. Khan, A., Singh, P. & Srivastava, A. Synthesis, nature and utility of universal iron chelator – Siderophore: A review. *Microbiol. Res.* **212–213**, 103–111 (2018).
78. Vandevivere, P., Welch, S. A., Ullman, W. J. & Kirchman, D. L. Enhanced dissolution of silicate minerals by bacteria at near-neutral pH. *Microb. Ecol.* **27**, 241–51 (1994).
79. Bennett, P. C., Rogers, J. R., Choi, W. J. & Hiebert, F. K. Silicates, Silicate Weathering, and Microbial Ecology. *Geomicrobiol. J.* **18**, 3–19 (2001).
80. Ullman, W. J., Kirchman, D. L., Welch, S. A. & Vandevivere, P. Laboratory evidence for microbially mediated silicate mineral dissolution nature. *Chem. Geol.* **132**, 11–17 (1996).
81. Welch, S. A., Barker, W. W. & Banfield, J. F. Microbial extracellular polysaccharides and plagioclase dissolution. *Geochim. Cosmochim. Acta* **63**, 1405–1419 (1999).
82. Marvasi, M. et al. Bacterial community analysis on the Mediaeval stained glass window "Natività" in the Florence Cathedral. *J. Cult. Herit.* **10**, 124–133 (2009).
83. Valbi, V. et al. Bacterial diversity on stained glass windows. *Int. Biodegradation. Biodegrad.* **177**, 105529 (2023).
84. Gentaz, L. Simulation Et Modelisation De L'Alteration Des Verres De Composition Medicale Dans L'Atmosphere Urbaine. (Université Paris-Est Créteil, 2011).
85. Nelson, C. & White, W. B. Transition metal ions in silicate melts—I. Manganese in sodium silicate melts. *Geochim. Cosmochim. Acta* **44**, 887–893 (1980).
86. Green, L. R. & Hart, F. A. Colour and chemical composition in ancient glass: An examination of some roman and wealden glass by means of ultraviolet-visible-infra-red spectrometry and electron microprobe analysis. *J. Archaeol. Sci.* **14**, 271–282 (1987).
87. Bidegaray, A.-I. et al. To be purple or not to be purple? How different production parameters influence colour and redox in manganese containing glass. *J. Archaeol. Sci. Rep.* **27**, 101975 (2019).
88. Good, N. E. et al. Hydrogen Ion Buffers for Biological Research. *Biochemistry* **5**, 467–477 (1966).

ACKNOWLEDGEMENTS

This work was supported by the Paris Ile-de-France Region – DIM “Matériaux anciens et patrimoniaux” and by the Doctoral school “Science Ingénierie et Environnement” of Université Paris-Est. The authors wish to thank Laura Galezowski and François Guyot from IMPMC for the supply of the bacteria strain and the fruitful discussions. The authors are also thankful to Céline Rommevaux for the wise advices.

AUTHOR CONTRIBUTIONS

S.R., A.V.C., and A.P. supervised the study. A.P. and V.V. designed the experiments. V.V. conducted the experiments and wrote the paper. All the authors helped in paper editing.

COMPETING INTERESTS

The authors declare that they have no known competing financial interests or personal relationships that could have appeared to influence the work reported in this paper.

ADDITIONAL INFORMATION

Supplementary information The online version contains supplementary material available at <https://doi.org/10.1038/s41529-023-00338-5>.

Correspondence and requests for materials should be addressed to Valentina Valbi.

Reprints and permission information is available at <http://www.nature.com/reprints>

Publisher's note Springer Nature remains neutral with regard to jurisdictional claims in published maps and institutional affiliations.



Open Access This article is licensed under a Creative Commons Attribution 4.0 International License, which permits use, sharing, adaptation, distribution and reproduction in any medium or format, as long as you give appropriate credit to the original author(s) and the source, provide a link to the Creative Commons license, and indicate if changes were made. The images or other third party material in this article are included in the article's Creative Commons license, unless indicated otherwise in a credit line to the material. If material is not included in the article's Creative Commons license and your intended use is not permitted by statutory regulation or exceeds the permitted use, you will need to obtain permission directly from the copyright holder. To view a copy of this license, visit <http://creativecommons.org/licenses/by/4.0/>.

© The Author(s) 2023